Intrinsic buckling strength of graphene: First-principles density functional theory calculations

Sandeep Kumar, K. P. S. S. Hembram, and Umesh V. Waghmare
Theoretical Sciences Unit, Jawaharlal Nehru Centre for Advanced Scientific Research, Jakkur Campus, Bangalore 560064, India
(Received 16 January 2010; revised manuscript received 24 July 2010; published 8 September 2010)

How graphene, an atomically thin two-dimensional crystal, explores the third spatial dimension by buckling under compression is not yet understood. Knowledge of graphene's buckling strength, the load at which it transforms from planar to buckled form, is a key to ensure mechanical stability of graphene-based nanoelectronic and nanocomposite devices. Here, we establish using first-principles theoretical analysis that graphene has an intrinsic rigidity against buckling, and it manifests in a weakly linear component in the dispersion of graphene's flexural acoustic mode, which is believed to be quadratic. Contrary to the expectation from the elastic plate theory, we predict within continuum analysis that a graphene monolayer of macroscopic size buckles at a nonzero critical compressive strain at $T=0$ K, and demonstrate it numerically from first principles. The origin of this rigidity is traced to the coupling between structural and electronic degrees of freedom arising from curvature-induced overlap between π orbitals in graphene.

DOI: 10.1103/PhysRevB.82.115411 PACS number(s): 61.48.Gh

I. INTRODUCTION

Graphene, a crystalline membrane marked by spectacular electronic properties and high structural strength,[1,2] is a very promising candidate for applications in nanoelectronics and nanocomposites.[3,4] However, such applications require deep understanding of graphene's structural response to external stresses, to thermal fluctuations and interaction with the substrate. Experimental and theoretical studies have demonstrated emergence of fracture instability in graphene under uniaxial tension.[1,5] The intrinsic strength of graphene against fracture, as reported in these studies, is highest among all materials. Bao *et al.* recently demonstrated how strain-induced ripples in graphene can be controlled via thermomechanical manipulation to allow device design based on strain engineering.[6] Underscored in their work is the need to develop a clear understanding of rippling in graphene under compression.

Stability of graphene as a strictly two-dimensional crystalline membrane has been a subject of theoretical debate in view of the Mermin-Wagner theorem, which argues for the lack of long-range order such as crystallinity in two dimensions at nonzero temperature in the absence of long-range interactions.[7] On the other hand, experimental isolation of free-standing graphene has demonstrated the existence of quasilong-range translational order in graphene at finite temperature.[8] Monte Carlo simulations based on highly accurate many-body interatomic potential showed that the topographical corrugations (ripples) arising from anharmonic coupling between long-wavelength stretching and bending modes stabilize the monolayer graphene against thermal fluctuations by deforming mesoscopically in the third dimension.[9]

Buckling of thin elastic membranes in response to compression results in structural modulations similar to ripples induced by thermal fluctuations.[10,11] Buckling of an elastic membrane is illustrative of generic bifurcation phenomenon where the membrane, when compressed beyond a certain critical strain, explores an energetically preferred state by collapsing in out-of-plane direction. The stretching energy in an elastic membrane is dictated by two-dimensional stretching modulus ($\frac{Yh}{2(1-\nu^2)}$) and scales as $\mathcal{E}_s \sim \frac{Yhl^2}{2(1-\nu^2)}$ whereas the bending energy, which is dictated by bending stiffness, scales as $\mathcal{E}_b \sim \frac{Yh^3}{12(1-\nu^2)}$ where Y is Young's modulus, ν is Poisson ratio, h is thickness, and l is typical length of the membrane.[12,13] The ratio $\mathcal{E}_b/\mathcal{E}_s \sim (h/l)^2$ determines the relative ease of bending over stretching, and hence dictates the critical strain at which emergence of buckling in a membrane occurs.[14] From elasticity theory of plates, we expect that a membrane has a *vanishing* critical strain in macroscopic limit, i.e., when its in-plane dimensions are much larger than the thickness ($h/l \to 0$).

In contrast to typical crystalline membranes, we demonstrate here that graphene exhibits a nonvanishing resistance against buckling in the macroscopic limit ($l \to \infty$), and it is an intrinsic property of graphene. This intrinsic strength of graphene against buckling is attributed to a nonvanishing out-of-plane shear rigidity which has a signature in the dispersion of its flexural acoustic phonons. Using a combination of first-principles calculations and continuum analysis, we elucidate how nonvanishing shear rigidity nontrivially alters the elastic stability of a thin membrane against buckling when compressed uniaxially.

II. COMPUTATIONAL DETAILS

Our calculations are based on first-principles density functional theory as implemented in the PWSCF simulation package,[15] with a generalized gradient approximation[16] to exchange correlation energy of electrons and ultrasoft pseudopotential[17] to represent interaction between ionic cores and valence electrons. Kohn-Sham wave functions were represented with a plane-wave basis with an energy cutoff of 35 Ry and a charge density with a cutoff 210 Ry. Integration over irreducible Brillouin zone for charge density and total energy was performed with a uniform mesh of $42 \times 42 \times 1$ mesh of k points and occupation numbers were smeared using Methfessel-Paxton scheme[18] with broadening of 0.01 Ry. Errors in the stresses and total energy due to basis-set size, smearing parameter, and k points are converged to less than 0.1 GPa and 0.01 Ry, respectively.

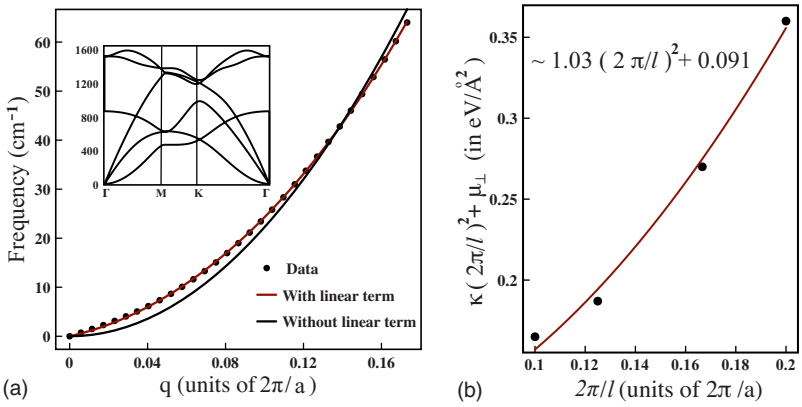

FIG. 1. (Color online) Left: dependence of ω_{flexural} on $\mathbf{q}$ in the vicinity of $\mathbf{q}=0$. Dots denote the data from first-principles lattice dynamics whereas the red/gray and black curves are second-order polynomial fits with and without the linear term, respectively. Excellent fitting in the presence of linear term should be noticed. Dispersion of phonons in unstrained graphene has been shown in inset. Right: effective rigidity of graphene, calculated from first-principles energetics, as a function of wave number $\frac{2\pi}{l}$, indicating a nonzero out-of-plane rigidity in accordance with lattice dynamics calculations.

III. RESULTS AND DISCUSSION

Oscillations of graphene with out-of-plane displacements of C atoms lead to two branches of phonons (one acoustic flexural and another optical). The acoustic flexural mode, due to translational and rotational symmetry of graphene, is believed to disperse as $\omega_{\text{flexural}}(\mathbf{q}) \propto \mathbf{q}^2$ as $\mathbf{q} \to 0$.[19] However, our lattice dynamics calculations based on linear-response theory demonstrate that acoustic flexural mode of graphene under uniaxial compressive strain, in the limit $\mathbf{q} \to 0$, has a behavior $\omega = k_1(\epsilon)|\mathbf{q}| + k_2(\epsilon)|\mathbf{q}|^2$ with $k_1(\epsilon=0) \neq 0$, $\mathbf{q}$ being the wave vector, and ϵ the applied strain (see Fig. 1). We have established that flexural phonon frequencies of unstrained graphene ($\epsilon=0$), particularly the coefficient of linear term, i.e., k_1, are converged with respect to k-point sampling with integration mesh finer than $36\times36\times1$ (see the Appendix).

Nonvanishing $k_1(\epsilon)$ at $\epsilon=0$ is indicative of nonzero shear modulus and hence a nonzero velocity of sound waves with out-of-plane polarization. Falkvosky recently obtained the dispersion of z-polarized acoustic phonon in graphene analytically using empirical interatomic force constants and reported a nonvanishing sound velocity in out-of-plane direction.[20] Sound velocities obtained from the two acoustic branches in longitudinal and transverse in-plane directions are in excellent agreement with values obtained from the experiments (see Table I). For the out-of-plane polarization, our estimate of sound velocity is 1.05 km/s as compared to 1.58 km/s reported by Falkovsky.[20]

Presence of a linear term in the transverse acoustic branch of a strictly two-dimensional membrane is believed to be prohibited since it violates the rotational invariance.[19] However, we show that a modification of continuum Hamiltonian is possible with an additional term to allow a linear component in the dispersion of z-polarized acoustic phonon without loss of rotational invariance. Graphene, in continuum limit, is modeled as a thin elastic sheet with bending rigidity κ, in-plane shear modulus μ, and Lame constant λ. The hexagonal symmetry of graphene lattice ensures the isotropy of its elastic properties and thus justifies the isotropic shell model. Deformed configuration of a membrane is described with two in-plane displacement fields u_1 and u_2, and a transverse displacement field w, which depend on the coordinate $\mathbf{r}=(x,y)$ of a planar reference state. Incorporating inputs from first-principles lattice dynamics and energetics into continuum analysis, we determine the form of the continuum Hamiltonian consistent with atomistics,

$$\mathcal{H} = \int\int_{\Omega} \left\{ \frac{\kappa}{2}[\nabla^2 w(x,y)]^2 + \mu \sum_{\alpha,\beta=1}^{2} \epsilon_{\alpha\beta}^2 + \frac{\lambda}{2}\left(\sum_{\alpha=1}^{2} \epsilon_{\alpha\alpha} \right)^2 - \frac{\mu_\perp}{2} w(x,y)\nabla^2 w(x,y) \right\} dxdy, \tag{1}$$

where the strain tensor $\{\epsilon_{\alpha\beta}\}$ is given as[14]

$$\epsilon_{\alpha\beta} = \frac{1}{2}\left[\frac{\partial u_\alpha}{\partial x_\beta} + \frac{\partial u_\beta}{\partial x_\alpha} + \frac{\partial w(x,y)}{\partial x_\alpha}\frac{\partial w(x,y)}{\partial x_\beta} \right]. \tag{2}$$

We notice that $\mathcal{H}$ is invariant under rigid body rotation and translation due to symmetry properties of ∇^2 and $\{\epsilon_{\alpha\beta}\}$. Our first-principles estimates of λ and μ are in excellent agreement with previous theoretical and experimental values (see Table II). κ and $\mu_\perp$ are determined from the first-principles estimate of energy cost associated with an out-of-plane sinusoidal deformation of graphene $[w(x) = \alpha \sin[\frac{2\pi x}{l}]]$ with respect to planar reference configuration of a $4n$-atom supercell, l being the length of the supercell and α being the amplitude of deformation wave. For this deformation and a uniaxial compression ϵ, continuum Hamiltonian assumes the form,

TABLE I. First-principles estimates of sound velocities compared with experimental estimates ($T \approx 300$ K) (Refs. 21 and 22).

	v_{LA} (km/s)	v_{TA} (km/s)	v_{ZA} (km/s)
Present	22.1	14.2	1.05
Experiments	24	14	

TABLE II. Mechanical properties of graphene calculated (first-principles) and earlier estimations (Refs. 1, 21, and 23).

	Y (eV/Å^2)	μ (eV/Å^2)	ν	λ (eV/Å^2)
Our estimations	20.2	8.8	0.16	3.0
Earlier estimations	21.20	9.1	0.14	2.0

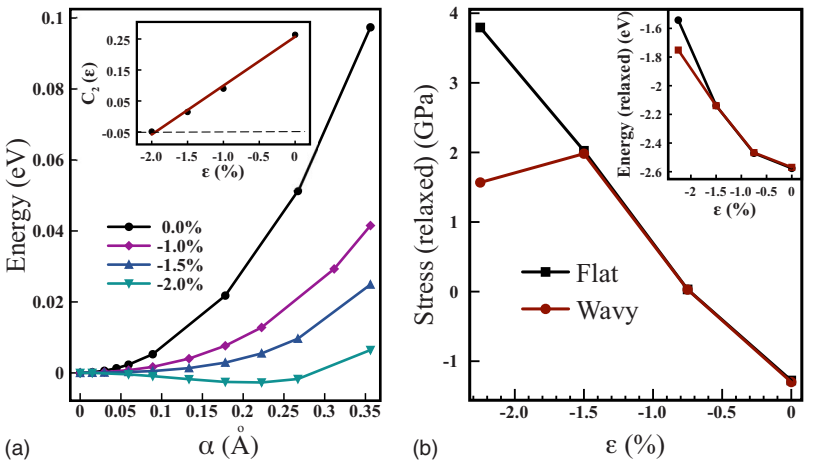

FIG. 2. (Color online) (a) Total energy (E) as a function of amplitude (α) calculated from first principles at various compressive strains. Diminishing slopes of E vs α^2 curves with compression indicate a buckling transition at $\epsilon=-1.5\%$. Shown in inset is variation in C_2, coefficient of α^2, with strain. (b) Stress vs strain and energy vs strain (inset) curves for graphene indicating the bifurcation at onset of buckling. Due to Pulay errors the stress values calculated at different strains are shifted with respect to their actual values by a small offset leading to apparent nonzero stress in undeformed state (Ref. 24).

$$\mathcal{H} = \frac{\sqrt{3}l^2(\lambda+2\mu)}{2n}\epsilon^2 + \frac{\sqrt{3}\pi^2}{n}\left[\left(\frac{2\pi}{l}\right)^2\kappa + \mu_\perp - (\lambda+2\mu)\epsilon\right]\alpha^2 + \frac{3\sqrt{3}\pi^4(\lambda+2\mu)}{4nl^2}\alpha^4. \quad (3)$$

The buckling instability, in this continuum model, occurs when $\frac{4\pi^2}{l^2}\kappa+\mu_\perp-(\lambda+2\mu)\epsilon\leq 0$. From this inequality, we notice that $\frac{4\pi^2}{l^2}\kappa+\mu_\perp$ is the effective rigidity against strain-induced buckling of a graphene sheet of length l. The contribution due to bending stiffness (κ) to effective rigidity diminishes as l^{-2}, and only $\mu_\perp$ contributes to the stability of a macroscopic graphene sheet. We consider four supercells comprising of 20, 24, 32, and 40 atoms with sinusoidal out-of-plane deformation and calculate their effective rigidities from first principles. From these values, we obtain the values of κ and $\mu_\perp$ as 1.03 eV and 0.091 eV/Å^2, respectively (see Fig. 1). Retaining only the harmonic terms in Fourier analysis of the continuum Hamiltonian (1), we obtain the dispersion of flexural acoustic mode as

$$\mathcal{H}(\mathbf{q}) \sim \frac{1}{2}m\omega_q^2 w_q^2 = \frac{1}{2}\{\kappa\mathbf{q}^4 + [\mu_\perp - (\lambda+2\mu)\epsilon]\mathbf{q}^2\}w_q^2. \quad (4)$$

Thus, we notice that a linear component in the dispersion of acoustic flexural phonons in unstrained graphene, i.e., $\epsilon=0$ arises from a nonvanishing $\mu_\perp$. Comparison of expression (5) with the first-principles lattice dynamics calculations provides us another way to independently deduce values of κ and $\mu_\perp$. κ and $\mu_\perp$ obtained from dispersion of acoustic flexural mode are 1.02 eV and 0.11 eV/Å^2, respectively, close to our earlier estimates. With these values of κ, μ, λ, and $\mu_\perp$, buckling of graphene for $n=6$ (24-atom supercell) is predicted to occur at the critical strain of −1.35%.

To validate this prediction of buckling transition from the continuum model, we carried out further first-principles total-energy calculations with a 24-atom supercell ($l=14.84$ Å) with out-of-plane sinusoidal deformation of different amplitudes. For small amplitude perturbations, the total energy of the perturbed structure varies as $E=E_{Flat}+C_2(\epsilon)\alpha^2+C_4(\epsilon)\alpha^4$, where the coefficients C_2 and C_4 are functions of applied in-plane strain ϵ. Stability of the structure with respect to out-of-plane perturbations is dictated by the sign of C_2, the coefficient of α^2. C_2 is observed to vary linearly with ϵ as expected from continuum theory, and becomes negative as graphene is compressed beyond a certain value indicating transition from planar to buckled state (see Fig. 2). This transition occurs at critical value of compressive strain of $\epsilon_{crit}\approx-1.5\%$ against $\epsilon_{crit}=-(\frac{4\pi^2}{l^2}\kappa+\mu_\perp)/(\lambda+2\mu)\approx-1.35\%$ as predicted by continuum analysis. In the macroscopic limit, i.e., $l\to\infty$, buckling occurs at a critical strain of $\epsilon_{crit}=-\mu_\perp/(\lambda+2\mu)\approx-0.5\%$. Lattice dynamics calculations carried out at increasing compressive strains indicate occurrence of long-wavelength instability between $\epsilon=-0.5\%$ and -0.75% (Fig. 3), corroborating the predictions of continuum theory.

The intrinsic buckling strength of graphene can be understood as arising from the stiffening action of the unhybridized π orbitals orienting normal to the plane of graphene. Our calculations verify that the Dirac point shifts along Γ-K direction from K point with small uniaxial strain and no band gap opens.[25] On out-of-plane deformation, the curvature alters the relative orientation of π orbitals, as shown in Fig. 4, leading to a change in overlap between neighboring π orbitals.[26] Our analysis for incipient buckling (see the Appendix) shows that π-π interactions in graphene lead to a term in the continuum Hamiltonian,

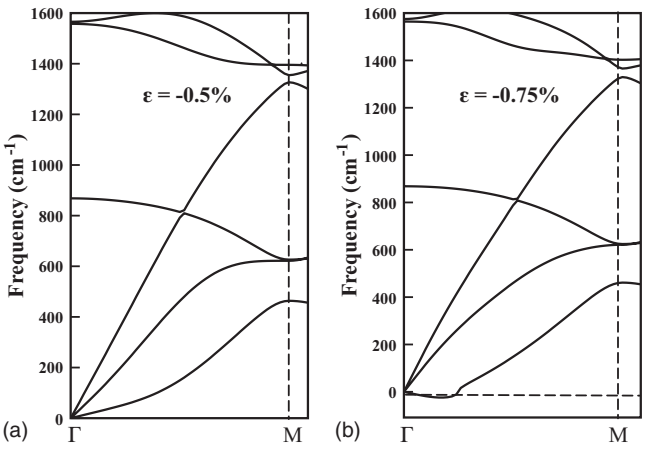

FIG. 3. (a) Phonon spectrum at $\epsilon=-0.5\%$. (b) Phonon spectrum at $\epsilon=-0.75\%$. Softening of z-transverse acoustic branch with strain should be noticed. Imaginary frequencies at $\epsilon=-0.75$ indicate a transverse structural instability as a result of compression.

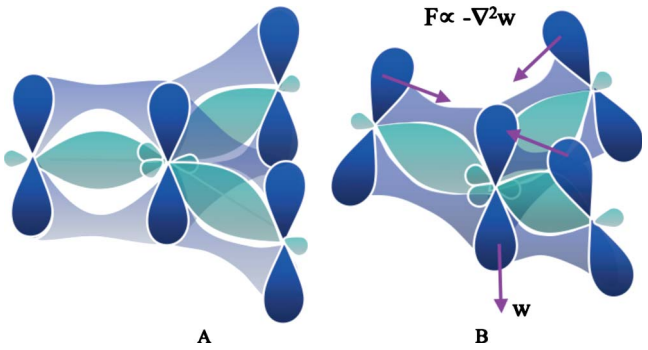

FIG. 4. (Color online) The force felt by a carbon atom pulled out of planar structure [shown in (a)] is proportional to the local curvature [$\nabla^2 w(\mathbf{r})$], that arises from the curvature-induced overlapping between π orbitals in graphene [shown in (b)]. The arrows indicate the relative tilting of π orbitals as graphene is deformed in out of plane direction.

$$\mathcal{H}_{\pi\text{-}\pi} = -\frac{\mu_\perp}{2}\int_{\mathcal{A}} w\nabla^2 w d\mathbf{r}, \tag{5}$$

where $\mathcal{A}$ indicates area of graphene sheet under consideration. This term vanishes for rigid body rotation of the membrane about *any* axis, respecting the rotational invariance (see the Appendix). Due to $\mathcal{H}_{\pi\text{-}\pi}$, an out-of-plane deformation $w(\mathbf{r})$ feels a restoring force $(\frac{\delta\mathcal{H}_{\pi\text{-}\pi}}{\delta w})$ that is proportional to local curvature, i.e., $\nabla^2 w$ (see Fig. 4). Under the boundary condition that the edges of the membrane are hinged against out-of-plane displacements, i.e., $w=0$ at the edges, we have

$$\mathcal{H}_{\pi\text{-}\pi} = \frac{\mu_\perp}{2}\int_{\mathcal{A}} (\nabla w)^2 d\mathbf{r}. \tag{6}$$

$\mathcal{H}_{\pi\text{-}\pi}$ can now be identified as strain energy contribution due to an out-of-plane shear of membrane, and $\mu_\perp$ as slope of flexural acoustic branch.

IV. SUMMARY

We have used a combination of first-principles theoretical and continuum analyses in exploration of buckling transition of graphene with uniaxial compressive in-plane strain. Contrary to the prediction of elastic plate theory, we predict that buckling of macroscopic graphene occurs at a nonzero compressive strain. This intrinsic buckling strength arises from curvature induced mixing among its π orbitals. Our first-principles continuum theory should be greatly useful in ensuring mechanical stability in design of graphene-based nanoelectronic devices and nanocomposites.

ACKNOWLEDGMENTS

S.K. and K.P.S.S. Hembram gratefully acknowledge financial support from CCMS/DST and DRDO, government of India, respectively. U.V.W. thanks DAE.

APPENDIX

1. Derivation of $\mathcal{H}_{\pi\text{-}\pi}=-\frac{\mu_\perp}{2}\int_{\mathcal{A}} w\nabla^2 w d\mathbf{r}$

Here we show that the additional $\mathcal{H}_{\pi\text{-}\pi}$ term in the continuum Hamiltonian arises due to curvature-induced π-π interaction. Let us consider an initially flat sheet of graphene in which all the π orbitals are oriented in the same direction [shown in Fig. 4(a)]. Pulling out a carbon atom in out-of-plane direction results in a local curvature and hence in a misalignment of neighboring π orbitals from unidirectional configuration [shown in Fig. 4(b)]. To obtain the mathematical form for curvature-induced π-π interaction, π orbitals are modeled as negatively charged skew rods in space. Electrostatic interaction between two charged skew rods, indexed as i and j, is described by a separable function of interaxial distance $r_{ij}=\sqrt{r_0^2+(w_j-w_i)^2}$ (r_0 is interaxial distance in flat state and w_j-w_i is relative vertical displacement) and angle of misalignment θ_{ij}.[27,28] The angle of misalignment between two skew lines is defined as the angle between any two lines parallel to them and passing through a point of space. Energy of curvature-induced π-π interaction can be generically written as

$$\mathcal{E}_{\pi\text{-}\pi} = \mathcal{F}(\sqrt{r_0^2+(w_j-w_i)^2})\mathcal{G}(\theta_{ij}) - \mathcal{F}_0\mathcal{G}_0 \tag{A1}$$

with $\mathcal{F}_0=\mathcal{F}(r=r_0)$ and $\mathcal{G}_0=\mathcal{G}(\theta_{ij}=0)$ so that the energy in the undeformed configuration is zero.

Energy due to interaction of ith π orbital with its neighboring π orbitals (considering only nearest-neighbor interactions) is

$$\mathcal{H}_i = \sum_{j=1}^{j=3}\mathcal{E}_{\pi\text{-}\pi} = \sum_{j=1}^{j=3}\mathcal{F}(\sqrt{r_0^2+(w_j-w_i)^2})\mathcal{G}(\theta_{ij}) - \mathcal{F}_0\mathcal{G}_0. \tag{A2}$$

Next we write Taylor-series expansions for the functions $\mathcal{F}$ and $\mathcal{G}$ in terms of their respective arguments. For incipient buckling, we can assume that w as well as ∇w is small. Therefore, in what follows, we retain only terms upto second power of ∇w. Further, it also should be noted that the higher-order derivative terms are higher order in $\mathbf{q}$, and the continuum limit corresponds to $\mathbf{q}\to 0$. Thus higher-order terms, i.e., $\nabla^n w(n>2)$ can be justifiably neglected,

$$\begin{aligned}\mathcal{F}(r) &= \mathcal{F}_0 + \left(\frac{\partial\mathcal{F}}{\partial r}\right)_{r_0}[\sqrt{r_0^2+(w_j-w_i)^2}-r_0] \\ &= \mathcal{F}_0 + \frac{1}{2r_0}\left(\frac{\partial\mathcal{F}}{\partial r}\right)_{r_0}(w_j-w_i)^2.\end{aligned} \tag{A3}$$

Substituting

$$w_j - w_i = \left(\frac{\partial w}{\partial x}\right)_i (x_j-x_i) + \left(\frac{\partial w}{\partial y}\right)_i (y_j-y_i), \tag{A4}$$

$$\mathcal{F}(r) = \mathcal{F}_0 + \frac{1}{2r_0}\left(\frac{\partial \mathcal{F}}{\partial r}\right)_{r_0}\left(\frac{\partial w}{\partial x}\right)_i^2 (x_j - x_i)^2 + \frac{1}{2r_0}\left(\frac{\partial \mathcal{F}}{\partial r}\right)_{r_0}\left(\frac{\partial w}{\partial y}\right)_i^2 (y_j - y_i)^2 + \frac{1}{r_0}\left(\frac{\partial \mathcal{F}}{\partial r}\right)_{r_0}\left(\frac{\partial w}{\partial x}\right)_i\left(\frac{\partial w}{\partial y}\right)_i (x_j - x_i)(y_j - y_i). \tag{A5}$$

Further terms in the Taylor expansion would contain powers of $\frac{\partial w}{\partial x}$ and $\frac{\partial w}{\partial y}$ higher than 2 and therefore have been neglected.

Substituting $(\frac{\partial \mathcal{F}}{\partial r})_{r_0}=0$ in Eq. (A5) we obtain

$$\mathcal{F}(\sqrt{r_0^2 + (w_j - w_i)^2}) \approx \mathcal{F}_0. \tag{A6}$$

Thus, $\mathcal{F}$ remains unchanged to second-order variation in ∇w. Next let us consider the Taylor expansion of angular dependence part, i.e., $\mathcal{G}(\theta_{ij})$ of deformation potential,

$$\mathcal{G}(\theta_{ij}) = \mathcal{G}_0 + \left(\frac{\partial \mathcal{G}}{\partial \theta_{ij}}\right)_{\theta_{ij}=0}\theta_{ij} + \frac{1}{2}\left(\frac{\partial^2 \mathcal{G}}{\partial \theta_{ij}^2}\right)_{\theta_{ij}=0}\theta_{ij}^2. \tag{A7}$$

For small deviation from reference flat state ($\theta_{ij}=0$), the angular function $\mathcal{G}(\theta_{ij})$ should vary quadratically with θ_{ij}, i.e., $\mathcal{G} \propto \theta_{ij}^2$. Therefore,

$$\left(\frac{\partial \mathcal{G}}{\partial \theta_{ij}}\right)_{\theta_{ij}=0} = 0. \tag{A8}$$

Thus

$$\mathcal{G}(\theta_{ij}) = \mathcal{G}_0 + \frac{1}{2}\left(\frac{\partial^2 \mathcal{G}}{\partial \theta_{ij}^2}\right)_{\theta_{ij}=0}\theta_{ij}^2. \tag{A9}$$

This is assumed in what follows that the magnitude of misalignment $|\theta_{ij}|$ is determined by magnitude of local gradient, i.e., $|\theta_{ij}| \sim |\nabla w_i|$. Substitution in Eq. (A9) yields,

$$\mathcal{G}(\theta_{ij}) = \mathcal{G}_0 + \frac{1}{2}\left(\frac{\partial^2 \mathcal{G}}{\partial \theta_{ij}^2}\right)_{\theta_{ij}=0}(\nabla w_i)^2. \tag{A10}$$

Substitution from Eqs. (A6) and (A9) in Eq. (A2) gives

$$\mathcal{H}_i = \frac{3}{2}\mathcal{F}_0\left(\frac{\partial^2 \mathcal{G}}{\partial \theta_{ij}^2}\right)_{\theta_{ij}=0}(\nabla w_i)^2. \tag{A11}$$

Let S_0 be the area per atom in the planar configuration while S_i be the projection of area per atom in deformed configuration on x-y plane. Then we can write total energy due to π-π interactions as

$$\mathcal{H}_{\pi\text{-}\pi} = \sum_i \frac{1}{S_0}\mathcal{H}_i S_i, \tag{A12}$$

$$= \sum_i \frac{3}{2}\frac{1}{S_0}\mathcal{F}_0\left(\frac{\partial^2 \mathcal{G}}{\partial \theta_{ij}^2}\right)_{\theta_{ij}=0}(\nabla w_i)^2 S_i. \tag{A13}$$

The continuum analog of which is

$$\mathcal{H}_{\pi\text{-}\pi} = \int_{\mathcal{A}} \frac{\mu_\perp}{2} dS(\nabla w)^2 \tag{A14}$$

with $\frac{\mu_\perp}{2} = \frac{1}{S_0}\frac{3}{2}\mathcal{F}_0(\frac{\partial^2 \mathcal{G}}{\partial \theta_{ij}^2})_{\theta_{ij}=0}$.

Under the boundary condition that the edges of the membrane are hinged against out of plane displacements, i.e., $w=0$ at the edges, Eq. (A14) becomes

$$\mathcal{H}_{\pi\text{-}\pi} = -\frac{\mu_\perp}{2}\int_{\mathcal{A}} d\mathbf{r} w \nabla^2 w. \tag{A15}$$

2. Invariance of $\mathcal{H}_{\pi\text{-}\pi}$ under symmetry operations

a. Translational Invariance

Out-of-plane displacement w is always measured relative to a flat reference configuration. Hence an overall rigid body translation of the sheet leaves the out-of-displacement field unchanged, and no alteration in $\mathcal{H}_{\pi\text{-}\pi}$ occurs. This straightforward leads to translational invariance.

b. Rotational Invariance

For a planar sheet, out-of-plane displacement field identically vanishes, i.e., $w \equiv 0$ and hence $\nabla^2 w \equiv 0$. We now show that a rigid body rotation of the graphene sheet about x or y axis does not cost any energy due to presence of $-\mu_\perp/2(w\nabla^2 w)$ term. Let us rotate the sheet about y axis by an arbitrary nonzero angle θ. Such a rotation results in a nonvanishing out-of-plane displacement field, i.e., $w = x \sin\theta$, $\nabla w = (\sin\theta, 0)$. However, we notice that a flat sheet remains flat under such a transformation, and hence we still have $\nabla^2 w = 0$. Thus we still have $-\mu_\perp/2(w\nabla^2 w) = 0$ implying that a rigid body rotation about an in-plane axis does not cost any energy. Even by integrating by parts, we arrive at the same conclusion as we show following:

$$\int_a^b w\frac{\partial^2 w}{\partial x^2}dx = w\frac{\partial w}{\partial x}\Big|_a^b - \int_a^b \left(\frac{\partial w}{\partial x}\right)^2 dx. \tag{A16}$$

Substituting $w = x\sin\theta$ and $\frac{\partial w}{\partial x} = \sin\theta$,

$$w\frac{\partial w}{\partial x}\Big|_a^b = (b-a)\sin^2\theta \tag{A17}$$

and

$$\int_a^b \left(\frac{\partial w}{\partial x}\right)^2 dx = (b-a)\sin^2\theta. \tag{A18}$$

Thus,

$$\int_a^b w\frac{\partial^2 w}{\partial x^2}dx = 0. \tag{A19}$$

Thus Hamiltonian remains invariant under rigid body rotation.

c. Reflection Invariance

Under reflection

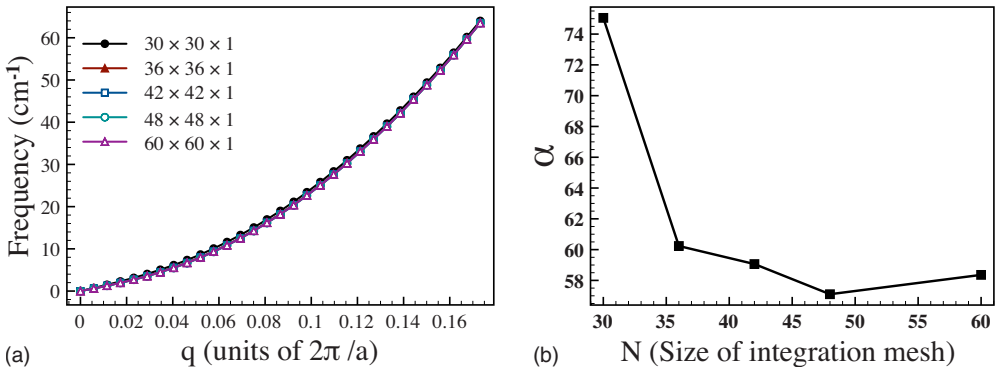

FIG. 5. (Color online) Left: convergence of phonon dispersion with the integration mesh. Notice that no change in phonon dispersion curves is noticed for integration mesh finer than $36\times36\times1$. Right: convergence of coefficient of linear term (α) with number of k points in the integration mesh ($N\times N\times1$).

$$w \to -w \quad \text{and} \quad \nabla^2 w \to -\nabla^2 w.$$

Therefore

$$(-w)(-\nabla^2 w) \to w\nabla^2 w \tag{A20}$$

Thus the invariance under reflection is maintained.

3. Force-displacement interpretation of $\mathcal{H}_{\pi\text{-}\pi}$

To understand the origin $\mathcal{H}_{\pi\text{-}\pi}$ from the force-displacement interpretation, we carry out the functional differentiation of $\mathcal{H}_{\pi\text{-}\pi}$ with respect to $w(x,y)$ to obtain the effective force,

$$F = -\frac{\delta\mathcal{H}_{\pi\text{-}\pi}[w(x,y)]}{\delta w(x',y')} = -\lim_{\epsilon\to0}\frac{\mathcal{H}_{\pi\text{-}\pi}[w(x,y)+\epsilon\delta(x-x',y-y')]-\mathcal{H}_{\pi\text{-}\pi}[w(x,y)]}{\epsilon} \tag{A21}$$

$$= \int_{\mathcal{A}} \frac{\mu_\perp}{2}\nabla^2 w(x,y)\,\delta(x-x',y-y')d\mathbf{r} + \int_{\mathcal{A}} \frac{\mu_\perp}{2}\nabla^2\delta(x-x',y-y')w(x,y)d\mathbf{r}$$

$$+ \lim_{\epsilon\to0}\epsilon\int_{\mathcal{A}} \frac{\mu_\perp}{2}\delta(x-x',y-y')\nabla^2\delta(x-x',y-y')d\mathbf{r}$$

$$= \int_{\mathcal{A}} \frac{\mu_\perp}{2}\nabla^2 w(x,y)\,\delta(x-x',y-y')d\mathbf{r} + \int_{\mathcal{A}} \frac{\mu_\perp}{2}\nabla^2\delta(x-x',y-y')w(x,y)d\mathbf{r}. \tag{A22}$$

Using the property of Dirac delta function, first term in the sum can be reduced as

$$\int_{\mathcal{A}} \frac{\mu_\perp}{2}\nabla^2 w(x,y)\,\delta(x-x',y-y')d\mathbf{r} = \frac{\mu_\perp}{2}\nabla^2 w(x',y'). \tag{A23}$$

Using integration by parts, we obtain reduction for second term as

$$\int_{\mathcal{A}} \frac{\mu_\perp}{2}\nabla^2\delta(x-x',y-y')w(x,y)d\mathbf{r} = \frac{\mu_\perp}{2}\nabla^2 w(x',y'). \tag{A24}$$

Hence, we obtain force as

$$F = \mu_\perp\nabla^2 w(x',y').$$

Thus, we deduce that due to $\mathcal{H}_{\pi\text{-}\pi}$, an out-of-plane deformation $w(\mathbf{r})$ feels a restoring force $(-\frac{\delta\mathcal{H}_{\pi\text{-}\pi}[w(x,y)]}{\delta w(x',y')})$ that is proportional to local curvature, i.e., $\nabla^2 w$.

4. Convergence of phonon frequencies with number of k points in the integration mesh

The convergence of phonon frequencies with number of k points in the integration mesh has been estimated. Our calculations indicate that phonon frequencies converge quite rapidly with number of k points in the integration mesh and there is almost no change in phonon dispersion curves for integration mesh finer than $36\times36\times1$ [see Fig. 5 (left)].

The acoustic phonons corresponding to each of these integration mesh is fitted to a polynomial of the type $\alpha q+\beta q^2$ and the coefficient of linear term, i.e., α is plotted with N (corresponding to a $N\times N\times 1$ integration mesh) [see Fig. 5 (right)]. The convergence of α with N to a nonzero value establishes genuine presence of linear term in the acoustic phonon of graphene and hence indicates nonvanishing buckling strength of graphene.

[1] C. Lee, X. Wei, J. Y. Kysar, and J. Hone, Science **321**, 385 (2008).
[2] A. K. Geim and K. S. Novoselov, Nature Mater. **6**, 183 (2007).
[3] W. Hill, A. K. Geim, K. Novoselov, F. Schedin, and P. Blake, IEEE Trans. Magn. **42**, 2694 (2006).
[4] S. Stankovich, D. A. Dikin, G. H. B. Dommett, K. M. Kohlhaas, E. J. Zimney, E. A. Stach, R. D. Piner, S. T. Nguyen, and R. S. Ruoffs, Nature (London) **442**, 282 (2006).
[5] F. Liu, P. Ming, and J. Li, Phys. Rev. B **76**, 064120 (2007).
[6] W. Bao, F. Miao, Z. Chen, H. Zhang, W. Jang, C. Dames, and C. N. Lau, Nat. Nanotechnol. **4**, 562 (2009).
[7] N. D. Mermin, Phys. Rev. **176**, 250 (1968).
[8] J. C. Meyer, A. K. Geim, M. I. Katsnelson, K. S. Novoselov, T. J. Booth, and S. Roth, Nature (London) **446**, 60 (2007).
[9] A. Fasolino, J. H. Los, and M. I. Katsnelson, Nature Mater. **6**, 858 (2007).
[10] D. Moldovan and L. Golubovic, Phys. Rev. E **60**, 4377 (1999).
[11] R. Lipowsky and M. Girardet, Phys. Rev. Lett. **65**, 2893 (1990).
[12] Y. Huang, J. Wu, and K. C. Hwang, Phys. Rev. B **74**, 245413 (2006).
[13] A. Boudaoud, P. Patricio, Y. Couder, and M. B. Amar, Nature (London) **407**, 718 (2000).
[14] L. D. Landau and E. M. Lifshitz, *Theory of Elasticity* (Pergamon Press, New York, 1986).
[15] S. Baroni, S. de Gironcoli, A. Dal Corso, and P. Gianozzi, http://www.pwscf.org
[16] J. P. Perdew, K. Burke, and M. Ernzerhof, Phys. Rev. Lett. **77**, 3865 (1996).
[17] D. Vanderbilt, Phys. Rev. B **41**, 7892(R) (1990).
[18] M. Methfessel and A. T. Paxton, Phys. Rev. B **40**, 3616 (1989).
[19] E. Mariani and F. von Oppen, Phys. Rev. Lett. **100**, 076801 (2008).
[20] L. A. Falkovsky, Phys. Lett. A **372**, 5189 (2008).
[21] D. Sánchez-Portal, E. Artacho, J. M. Soler, A. Rubio, and P. Ordejón, Phys. Rev. B **59**, 12678 (1999).
[22] C. Oshima, T. Aizawa, R. Souda, Y. Ishizawa, and Y. Sumiyoshi, Solid State Commun. **65**, 1601 (1988).
[23] O. L. Blakslee, D. G. Proctor, E. J. Seldin, G. B. Spence, and T. Weng, J. Appl. Phys. **41**, 3373 (1970).
[24] G. P. Francis and M. C. Payne, J. Phys.: Condens. Matter **2**, 4395 (1990).
[25] T. O. Wehling, A. V. Balatsky, A. M. Tsvelik, M. I. Katsnelson, and A. I. Lichtenstein, EPL **84**, 17003 (2008).
[26] E. A. Kim and A. H. C. Neto, EPL **84**, 57007 (2008).
[27] D. Chapot, L. Bocquet, and E. Trizac, J. Chem. Phys. **120**, 3969 (2004).
[28] S. L. Brenner and V. A. Parsegian, Biophys. J. **14**, 327 (1974).